

Pharmacological profiling of a berbamine derivative for lymphoma treatment

Senlin Xu,^{1,2,*} Shunquan Wu,^{1,3,*} Mingfeng Zhang,¹ Jun Xie,⁴ Min Lin,⁴ Lihua Jin,¹ Jiawei Zhang,⁵ Yangmeng Wang,¹ Mingjie Fan,¹ Zhipeng Fang,¹ Weini Li,¹ Ching Ouyang,⁶ David Kwon,⁴ Natalie Que,⁷ Zhirou Li,⁸ Jinge Mao,⁸ Haonan Chen,⁷ Josephine Harris,¹ Xiwei Wu,⁶ Jun Wu,⁹ Hongwei Yin,⁴ Wing C. Chan,^{2,10} David Horne,^{2,4} and Wendong Huang^{1,2}

¹Molecular and Cellular Biology of Cancer Program and Department of Diabetes Complications and Metabolism, Arthur Riggs Diabetes and Metabolic Research Institute and ²Irell and Manella Graduate School of Biological Sciences, Beckman Research Institute, City of Hope, Duarte, CA; ³Department of Hematology, Fujian Institute of Hematology, Fujian Provincial Key Laboratory on Hematology, Fujian Medical University Union Hospital, Fujian, China; ⁴Department of Molecular Medicine, Beckman Research Institute, City of Hope National Medical Center, Duarte, CA; ⁵Cancer Institute (Key Laboratory of Cancer Prevention and Intervention, China National Ministry of Education), Second Affiliated Hospital, School of Medicine, Zhejiang University, Hangzhou, China; ⁶Integrative Genomic Core, City of Hope National Medical Center, Duarte, CA; ⁷Eugene and Ruth Roberts Summer Student Academy, City of Hope, Duarte, CA; ⁸School of AI and Advanced Computing, Xi'an Jiaotong-Liverpool University, Suzhou, Jiangsu, China; and ⁹Animal Tumor Model Core and ¹⁰Department of Pathology, City of Hope National Medical Center, Duarte, CA

Key Points

- PA4 is a potent CAMKII γ inhibitor.
- In vivo efficacy, pharmacokinetic, and toxicity assays suggest that PA4 is a candidate for future drug development.

Ca²⁺/calmodulin-dependent protein kinase II γ (CAMKII γ) has been identified as a potential target for treating cancer. Based on our previous study of berbamine (BBM) as a CAMKII γ inhibitor, we have synthesized a new BBM derivative termed PA4. Compared with BBM, PA4 showed improved potency and specificity and was more cytotoxic against lymphoma and leukemia than against other types of cancer. In addition to indirectly targeting c-Myc protein stability, we demonstrated that its cytotoxic effects were also mediated via increased reactive oxygen species production in lymphoma cells. PA4 significantly impeded tumor growth in vivo in a xenograft T-cell lymphoma mouse model. Pharmacokinetics studies demonstrated quick absorption into plasma after oral administration, with a maximum concentration of 1680 \pm 479 ng/mL at 5.33 \pm 2.31 hours. The calculated oral absolute bioavailability was 34.1%. Toxicity assessment of PA4 showed that the therapeutic window used in our experiments was safe for future development. Given its efficacy, safety, and favorable pharmacokinetic profile, PA4 is a potential lead candidate for treating lymphoma.

Introduction

The family of multifunctional serine/threonine kinases known as calcium/calmodulin (CaM) kinase II (CAMKII) comprises 4 isoforms, which are derived from alternative splicing of individual genes¹: CAMKII α , CAMKII β , CAMKII δ , and CAMKII γ . Expression of CAMKII α and CAMKII β are mostly limited to the brain, whereas CAMKII δ and CAMKII γ are widely expressed in peripheral tissues.² Recently, CAMKII has been reported to regulate cellular proliferation,³ modulate oncogenic pathways,⁴ and control cell cycle⁵ and is also implicated in cellular death pathways.⁶ Aberrant CAMKII expression and the tumor-promoting functions of CAMKII have been rigorously investigated in several solid tumors,

Submitted 28 June 2023; accepted 26 October 2023; prepublished online on *Blood Advances* First Edition 15 November 2023; final version published online 10 January 2024. <https://doi.org/10.1182/bloodadvances.2023010873>.

*S.X. and S.W. contributed equally to this study.

The RNA sequencing data are deposited in the Gene Expression Omnibus database (accession number GSE245491).

Other forms of data are available on request from the corresponding author, Wendong Huang (whuang@coh.org).

The full-text version of this article contains a data supplement.

© 2024 by The American Society of Hematology. Licensed under [Creative Commons Attribution-NonCommercial-NoDerivatives 4.0 International \(CC BY-NC-ND 4.0\)](https://creativecommons.org/licenses/by-nc-nd/4.0/), permitting only noncommercial, nonderivative use with attribution. All other rights reserved.

including osteosarcoma, head and neck squamous cell carcinoma, breast cancer, liver cancer, colon cancer, glioblastoma, and lung cancer.⁷⁻¹³ Activation of CAMKII also contributes to metastasis of breast cancer¹⁴ and drug resistance in ovarian cancer.¹⁵ Previous studies by our group have shown that 1 CAMKII isoform, CAMKII γ , plays a critical role in promoting the development of hematopoietic cancers. CAMKII γ is overexpressed in leukemia stem cells and promotes chronic myeloid leukemia.¹⁶ Activation of CAMKII γ also potentiates T-cell acute lymphoblastic leukemia leukemogenesis.¹⁷ Besides leukemia, CAMKII γ strongly promotes T-cell lymphoma by enhancing c-Myc protein stability and forming a synthetic lethality with c-Myc in lymphoma cells.¹⁸ These studies prompt us to develop CAMKII inhibitors for cancer treatment.

CAMKII is evolutionarily conserved in eukaryotic cells and shares similar functions in humans and mice.¹⁹ The kinase is composed of 3 domains. The N-terminal is the catalytic domain responsible for the catalytic activity. The regulatory domain in the middle binds to calcium and CaM. The association domain in the C-terminal forms either homopolymers or heteropolymers with other CAMKII proteins.²⁰ Calcium and CaM can directly activate CAMKII kinases by binding to the regulatory domain, leading to the phosphorylation of T286/287.²¹ The further autonomous phosphorylation of T286/287 results in Ca²⁺/CaM-independent activation.²² Afterward, a conformation change allows adenosine triphosphate (ATP) to bind to the catalytic domain. After that, substrate proteins enter the catalytic pocket of CAMKII kinases for further phosphorylation.

Because of the emerging roles of CAMKII in a wide spectrum of diseases, much effort has been devoted to developing CAMKII inhibitors, but none have yet been translated into the clinic. For instance, the small molecule KN-93 has been widely used in basic research.²³ It disrupts the binding of CaM to the regulatory domain of CAMKII but cannot inhibit CAMKII autonomous activity. Other efforts to develop CAMKII inhibitors have been based on small molecule nitrogen heterocycles: pyrimidines (Scios 15b, AS105),²⁴ 4-azabenzamidozoles (GS-680),²⁵ and thienopyrimidines (RA306).²⁶ These pyrimidine-based ATP-competitive inhibitors target CAMKII isoforms in cardiac tissue, but their roles in cancers are limited.

Given the role CAMKII γ plays in tumorigenesis, we have identified a natural compound berbamine (BBM) as a specific CAMKII γ inhibitor.¹⁶ BBM is a bisbenzylisoquinoline, isolated from the plant *Berberis amurensis*. Previously, it has been used to treat leukopenia after chemotherapy and radiation. We have studied its anti-tumor effects and therapeutic efficacy against chronic myeloid leukemia and T-cell lymphoma.^{16,18} Derivatives of BBM have also produced encouraging results in treating multiple cancers.²⁷⁻³⁰ However, the effective dosages and medicinal characteristics of those derivatives still need improvement for potential clinical applications.

In this study, we have assessed the antitumor efficacy, pharmacokinetic, and safety characteristics of PA4, a potent derivative of BBM that achieves desirable anticancer activity both in vitro and in vivo. Using PA4, we also identified a new cytotoxic mechanism of CAMKII γ inhibition in lymphoma cells. Given its improved efficacy, favorable pharmacokinetic profile, and safety, PA4 is a potential lead candidate for treating lymphoma and other cancers.

Methods

Cell lines and reagents

Cells were cultured with RPMI 1640 under standard culture conditions. SK-MEL-2 was cultured in Eagle's minimum essential medium. BBM and PA4 were dissolved in stock solutions with dimethyl sulfoxide (DMSO; Santa Cruz) at 10 mM for in vitro cell treatment. BBM and PA4 were dissolved in 1 × phosphate-buffered saline (PBS) for in vivo oral gavage.

CETSA

Cellular thermal shift assay (CETSA) was used to evaluate the interactions of PA4 and CAMKII γ in cells following a previously published protocol.³¹

Mouse xenograft model study

All animal procedures were approved by the institutional animal care and use committee at City of Hope. Eight-week-old NSG (NOD.Cg-Prkdcscid Il2rgtm1Wj/SzJ) mice were purchased from The Jackson Laboratory (strain no. 005557). H9 cells (5×10^6) suspended in 1 × PBS were injected subcutaneously in the right flank of female NSG mice. After the xenografted tumors reached a volume of ~30 mm³, the mice were randomized to 5 groups: (1) PBS: 100 μ L per day, n = 5; (2) BBM: 50 mg/kg per day (100 μ L), n = 5; (3) PA4: 5 mg/kg per day (100 μ L), n = 5; (4) PA4: 10 mg/kg per day (100 μ L), n = 5; and (5) PA4: 15 mg/kg per day (100 μ L), n = 5. PA4 was administered via oral gavage once a day for 14 days. Tumors and body weight were measured 3 times a week. Tumors were measured with Vernier calipers, and the tumor volume (mm³) was calculated as "length × width² / 2." Mice were euthanized on day 30 of inoculation, and tumor tissues were collected. Blood samples were obtained by cardiac puncture. Serum was separated by centrifugation and was further stored at -80°C until analysis. PA4 concentrations in serum and tumor tissues were analyzed by Integrated Analytical Solutions, Inc (Berkeley, CA) using liquid chromatography with tandem mass spectrometry.

Cell survival/proliferation assay

The 3-(4,5 dimethylthiazol-2-yl)-5-(3-carboxymethoxyphenyl)-2-(4-sulfophenyl)-2H-tetrazolium assay was conducted with the Cell-Titer 96 Aqueous Cell Proliferation Kit (Promega, Madison, WI). The 50% inhibitory concentration (IC₅₀) was defined as the drug concentration that induced a 50% viability decrease.

In vitro kinase assay

In vitro profiling using a 371-kinase panel was performed at Reaction Biology Corporation using the HotSpot assay platform.³²

Additional methods

Detailed methods of CETSA, differential scanning fluorimetry (DSF), RNA sequencing, western blot assay, flow cytometry, immunohistochemical analysis, in vitro kinase assay, mouse toxicity, and pharmacokinetics study are presented in supplemental Methods.

Statistical analysis

Student *t* test (2-sided) was applied, and changes were considered statistically significant for *P* < .05. In the figures, changes are noted using **P* < .05 and ***P* < .01. The data were normally distributed.

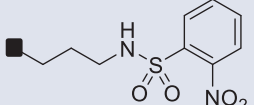
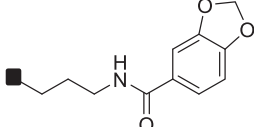
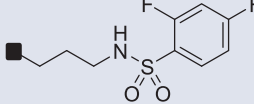
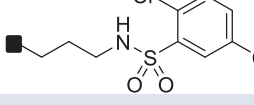
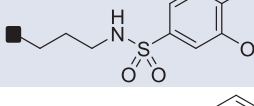
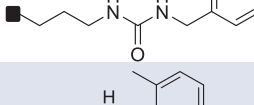
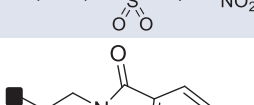
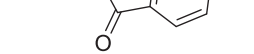
Variation within and between groups was not estimated. The sample size was not preselected, and there were no inclusion/exclusion criteria being used. The data shown in the bar graphs are the mean and standard deviation or standard error of the mean of at least 3 biological replicates. Statistical analysis was conducted using the GraphPad Prism software packages.

Results

Synthesis and characterization of PA4 as a potent inhibitor for CAMKII γ

Based on the initial hit, we synthesized 8 BBM derivatives and tested the cytotoxicity against lymphoma cell line H9. Of them, PA1, PA4, and PA7 were the top 3 inhibitors of cell growth (Table 1). Because the structures of PA1 and PA7 contain a nitro group, which has been extensively associated with mutagenicity and genotoxicity and is often categorized as a structural alert or a toxicophore,³³ we selected PA4 as our lead candidate. The structure of PA4 is shown in supplemental Figure 1A. Like BBM, PA4 may bind to the ATP pocket of CAMKII γ .³⁴ BBM was identified as a CAMKII γ inhibitor. To compare the target binding affinity of PA4, we first conducted CETSA using T-cell lymphoma H9 cells

Table 1. The IC₅₀ of BBM derivatives PA1-8

Derivatives	-R	IC ₅₀ (μ M)
PA1		0.74
PA2		1.26
PA3		0.95
PA4		0.76
PA5		1.83
PA6		1.80
PA7		0.82
PA8		3.74

(Figure 1A). In this assay, unbound proteins were denatured and precipitated by elevated temperatures, whereas drug-bound proteins remained in the solution. As shown in Figure 1B-C, CAMKII γ began to degrade at 47°C in the DMSO-treated (control) group. However, incubation of cells with 5 μ M PA4 for 1 hour significantly increased the degradation temperature at 47°C and 53°C (Figure 1B-C). These results suggest that PA4 stabilizes CAMKII γ . In contrast, 5 μ M of BBM did not shift the degradation temperature (Figure 1B-C). In addition, PA4 increased CAMKII γ thermal stability in a dose-dependent manner at 50°C (Figure 1D-E), whereas BBM did not (supplemental Figure 1B). These results revealed that PA4 binds to CAMKII γ and enhances its thermal stabilization at the cellular level.

We then used nano-DSF assay to further determine the physical binding of BBM or PA4 to purified CAMKII γ protein in vitro. Unlike conventional DSF, which uses a hydrophobic fluorescent dye, nano-DSF measures the changes in intrinsic protein fluorescence as the protein unfolds. Although incubation with BBM did not significantly change the melting temperature of CAMKII γ protein, PA4 incubation significantly induced a thermal shift, suggesting a physical binding between PA4 and CAMKII γ (Figure 1F).

The binding of PA4 with CAMKII γ resulted in significantly decreased kinase activity. We performed a kinome screening of both BBM and PA4 at concentrations of 1 μ M and 10 μ M. Of the entire panel of 371 kinases tested, none of the kinases' activity was reduced by >50% when treated with 10 μ M BBM. In contrast, 17 kinases were "hits" of PA4 at 10 μ M, and CAMKII γ was the top kinase based on the inhibitory percentage (Figure 2A). We then performed an in vitro kinase assay to determine the IC₅₀ values of PA4 for CAMKII γ . PA4 was more potent than BBM to inhibit CAMKII γ activity, with an IC₅₀ ~2.77 μ M in this assay (Figure 2B). Considering that PA4 may target other kinases, such as Bruton tyrosine kinase and zeta (ζ)-chain associated protein kinase 70 kDa (ZAP-70), which are also essential for lymphoma survival.³⁵ PA4 treatment slightly decreased the phosphorylation of interleukin-2-inducible T-cell kinase, the downstream signal of ZAP-70 in H9 cells (supplemental Figure 1C).

PA4 preferentially targeted hematological cancers

Next, we determined the activation of CAMKII γ in a wide spectrum of cancers. Phosphorylation at T287 is marked as CAMKII γ activation. We analyzed the CAMKII γ T287 phosphorylation vs total protein level based on the Cancer Proteogenomic Data Analysis Site data set. Breast cancer and stomach cancer were excluded because of a lack of healthy tissue data. Among the remaining 9 types of cancers, CAMKII γ T287 phosphorylation was significantly elevated in colon cancer, liver cancer, lung adenocarcinoma, and pancreatic ductal adenocarcinoma (Figure 3A).

To determine the cytotoxic effects of PA4, we screened it against the the US National Cancer Institute-60 human tumor cell line anticancer drug screen (NCI-60) panel of human tumor cell lines. We tested how BBM and PA4 affected 60 tumor cell lines from NCI-60 plus 6 pancreatic tumor and 5 lymphoma cell lines over 72 hours. The IC₅₀ values are presented in Table 2. Across all the cell lines that we screened, PA4 (vs BBM) demonstrated more cytotoxicity (Figure 3B). When we compared its effect among different types of cancers, hematological cell lines were more sensitive to PA4 (Figure 3B-C). Cells with higher CAMKII γ T287

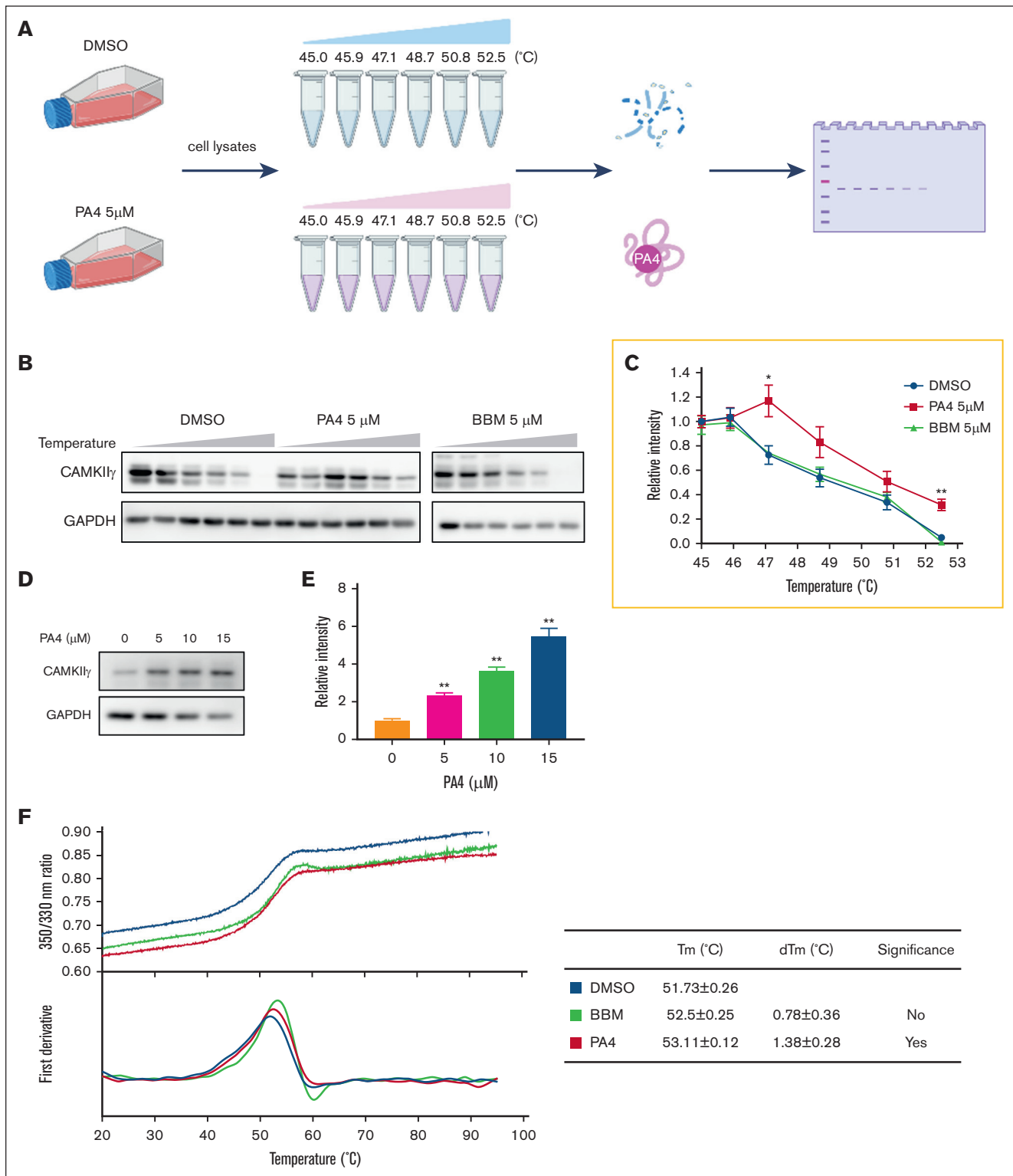


Figure 1. PA4 is a potent CAMKII γ inhibitor. (A) Scheme of CETSA assay. (B) H9 cells were treated with DMSO or 5 μ M PA4 for 1 hour. Next, the cells were collected in PBS and heated from 45°C to 52.5°C. Then, the proteins were extracted and subjected to western blot analysis of indicated proteins expression level. (C) The quantitative analysis of CAMKII γ shown in panel B. (D) H9 cells were pretreated with 0, 5, 10, or 15 μ M PA4 for 1 hour and then heated at 55°C. The western blot analysis of CAMKII γ expression level. (E) The quantitative analysis of CAMKII γ expression level from panel D. Data were expressed as mean \pm standard deviation (SD), $n = 3$; * $P < .05$ and ** $P < .01$ vs DMSO treatment. (F) The ratio of fluorescence 350:330 nm and the first derivatives of the transition curves from nano-DSF assay were plotted against the temperature. The melting temperature (Tm) values are derived from the maxima of the obtained first derivative curves. dTm, deviation of Tm.

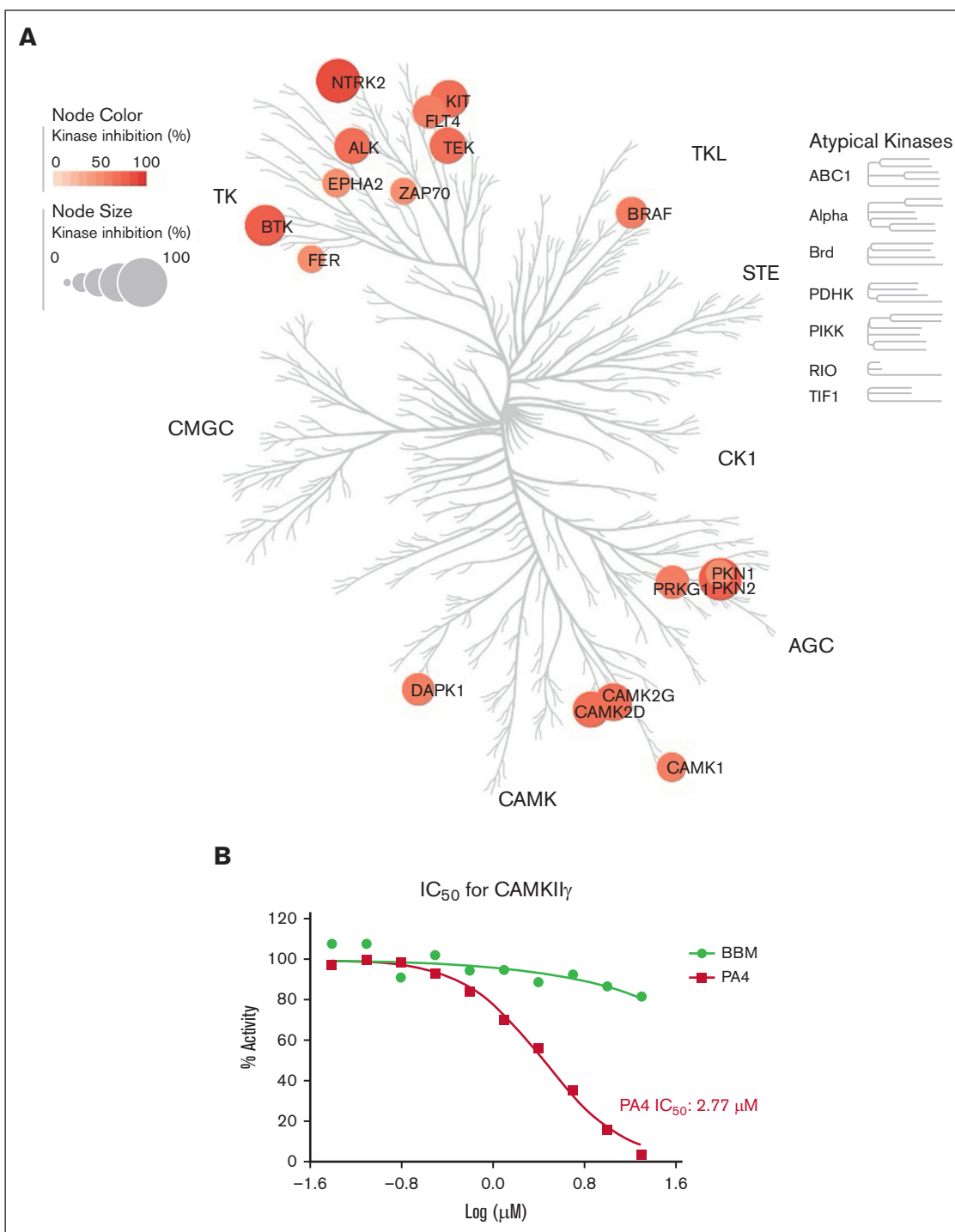


Figure 2. PA4 inhibits CAMKI γ kinase activity. (A) Kinase map of 17 kinases whose activities have been inhibited by $\geq 50\%$ by 10 μ M PA4 using in vitro kinome screening against a 371-kinase panel. (B) CAMKI γ kinase activity after incubation with either BBM or PA4 was determined by in vitro kinase assay. The kinase activity was expressed as the percent remaining kinase activity in test samples compared with vehicle (DMSO) reactions. IC₅₀ values and curve fits were obtained using Prism (GraphPad Software). ABC, activity of bc1 complex kinase group; AGC, a group of kinases containing PKA (protein kinase A), PKG, PKC families; ALK, anaplastic lymphoma kinase; BRAF, serine/threonine-protein kinase B-raf; BTK, Bruton's tyrosine kinase; CAMK, Ca²⁺/calmodulin-dependent protein kinase; CK1, casein kinase 1; CMGC, cyclin-dependent kinase [CDK], mitogen-activated protein kinase [MAPK], glycogen synthase kinase [GSK3], CDC-like kinase [CLK] protein kinases group including; DAPK1, death-associated protein kinase 1; EPHA, receptor tyrosine kinase; FER, FERON1; FLT, Fms related receptor tyrosine kinase; KIT, receptor tyrosine kinase type III; PDHK, Pyruvate dehydrogenase kinase; PIKK, phosphatidylinositol 3-kinase-related kinases; PKN, serine/threonine-protein kinase N1; PRKG1, protein kinase CGMP-dependent 1; RIO, a group of kinases containing the conserved RIO (right open reading frame) domain; STE, group of kinases containing homologs of yeast sterile 7, sterile 11, sterile 20 kinases; TEK, receptor tyrosine kinase; TIF, transcriptional intermediary factor; TKL, tyrosine kinase-like.

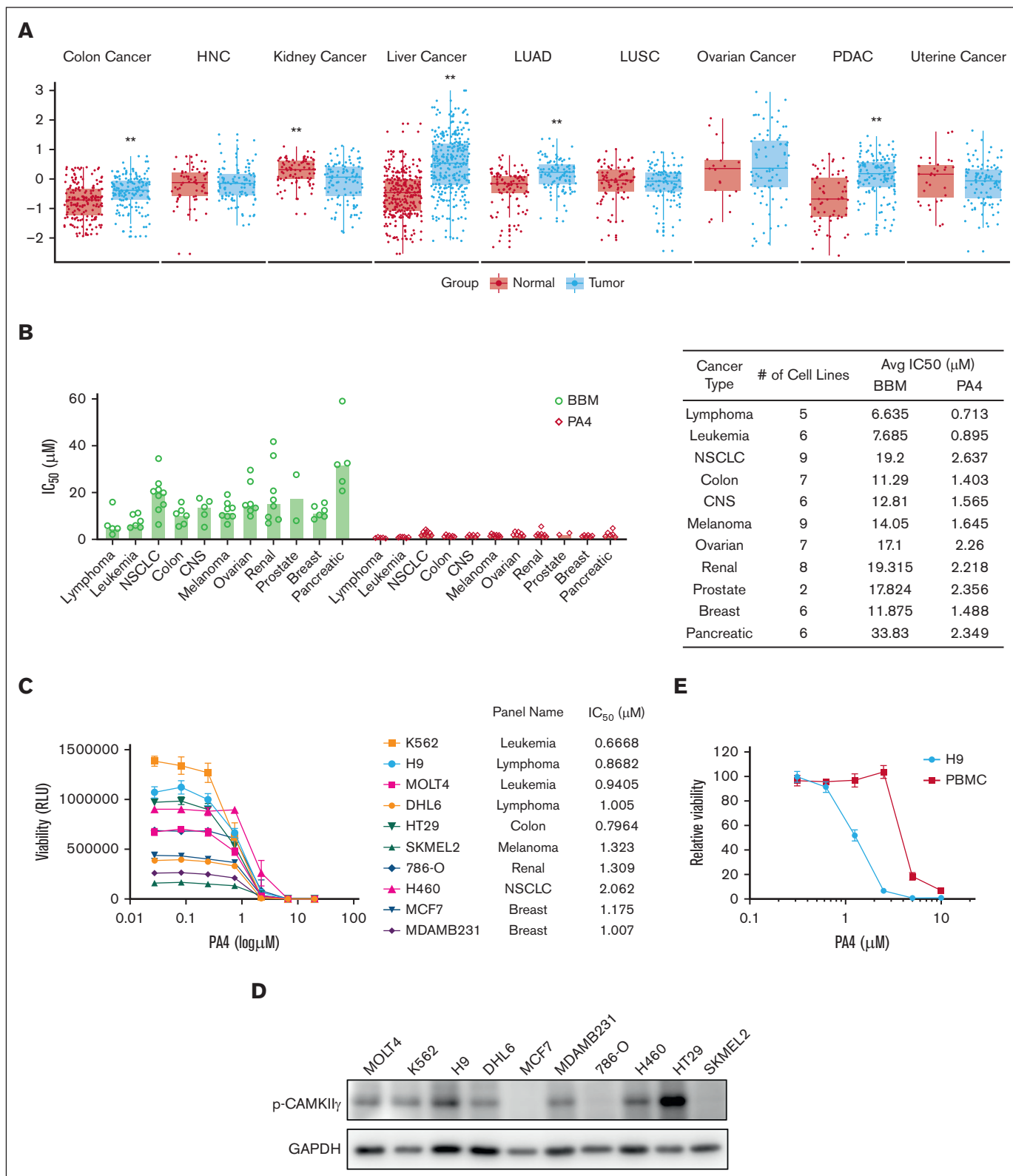


Figure 3. PA4 preferentially targets hematological cancers. (A) Box plots of CAMKIIγ T287 phosphorylation/total protein level among 9 types of cancers from the cProSite database; ** $P < .01$. (B) Summary of IC₅₀ of BBM or PA4 in cancer-derived cell lines treated with BBM or PA4 for 72 hours. Data are shown as individual values with median. (C) Summary of IC₅₀ of BBM or PA4 in 10 selected cell lines treated with PA4 for 72 hours. (D) Relative viability of H9 and human peripheral blood mononuclear cells (PBMCs) incubated with indicated dosages of PA4 for 24 hours. (E) CAMKIIγ T287 phosphorylation level among 10 selected cell lines from panel C was measured by western blot. Glyceraldehyde-3-phosphate dehydrogenase (GAPDH) was used as loading control. Avg, average; CNS, central nervous system; HNC, head and neck cancer; LUAD, lung adenocarcinoma; LUSC, lung squamous cell carcinoma; NSCLC, non-small cell lung cancer; PDAC, pancreatic adenocarcinoma; RLU, relative light unit.

Table 2. IC₅₀ of BBM and PA4 on NCI-60 panel of human tumor cell lines

Cell line	Panel name	IC ₅₀ (μM)	
		BBM	PA4
RPMI-8226	Leukemia	7.835	0.9439
K-562	Leukemia	5.112	0.768
MOLT-4	Leukemia	10.69	1.134
HL-60(TB)	Leukemia	5.976	0.9964
CCRF-CEM	Leukemia	11.36	1.007
SR	Leukemia	5.137	0.5188
A549/ATCC	Non-small cell lung	18.71	2.777
NCI-H460	Non-small cell lung	20.53	1.806
EKVX	Non-small cell lung	6.376	1.427
NCI-H522	Non-small cell lung	21.28	2.111
HOP-62	Non-small cell lung	23.82	4.233
NCI-H322M	Non-small cell lung	19.96	3.144
HOP-92	Non-small cell lung	12.71	2.792
NCI-H23	Non-small cell lung	14.9	1.779
NCI-H226	Non-small cell lung	34.55	3.662
SW-620	Colon	12.41	1.163
HT29	Colon	6.564	1.035
KM12	Colon	17.3	2.158
HCT-116	Colon	10.15	1.679
HCT-15	Colon	11.04	1.402
COLO 205	Colon	15.95	1.27
HCC-2998	Colon	5.606	1.114
SF-268	CNS	13.82	1.986
U251	CNS	10.66	1.125
SF-295	CNS	13.32	1.918
SNB-19	CNS	16.21	1.866
SNB-75	CNS	17.59	1.398
SF-539	CNS	5.252	1.098
MALME-3M	Melanoma	9.824	1.423
SK-MEL-2	Melanoma	16.01	1.038
LOX IMVI	Melanoma	23.04	1.76
SK-MEL-28	Melanoma	15.39	2.467
SK-MEL-5	Melanoma	9.896	1.306
M14	Melanoma	13.06	1.88
MDA-MB-435	Melanoma	13.46	1.819
UACC-257	Melanoma	6.497	1.17
UACC-62	Melanoma	19.23	1.941
NCI/ADR-RES	Ovarian	24.81	3.248
OVCAR-3	Ovarian	12.26	2.293
SK-OV-3	Ovarian	13.42	1.455
IGR-OV1	Ovarian	29.59	3.384
OVCAR-4	Ovarian	15.11	2.058
OVCAR-5	Ovarian	9.876	1.411
OVCAR-8	Ovarian	14.61	1.974
ACHN	Renal	20.78	2.318
UO-31	Renal	9.613	1.081

Table 2 (continued)

Cell line	Panel name	IC ₅₀ (μM)	
		BBM	PA4
786-0	Renal	8.476	1.242
SN12C	Renal	41.8	5.512
CAKI-1	Renal	14.23	1.765
TK-10	Renal	35.75	2.311
RXF 393	Renal	16.9	1.916
A498	Renal	6.971	1.602
PC-3	Prostate	7.938	1.98
DU-145	Prostate	27.71	2.732
MCF7	Breast	9.927	1.784
HS 578T	Breast	12.4	1.339
MDA-MB-468	Breast	10.4	1.528
MDA-MB-231/ATCC	Breast	14.16	1.265
BT-549	Breast	8.641	1.208
T-47D	Breast	15.72	1.801
FG	Pancreatic	32.59	2.176
BxPC3	Pancreatic	31.94	1.887
Su8686	Pancreatic	NA	1.263
Miapaca2	Pancreatic	20.72	1.122
Panc1	Pancreatic	24.78	2.866
CaPan2	Pancreatic	59.1	4.782
Rael	Lymphoma	5.874	0.6174
H9	Lymphoma	4.668	0.8066
Namalwa	Lymphoma	20.71	2.313
JB6	Lymphoma	2.119	0.7317
DHL6	Lymphoma	15.88	1.018
Mutu	Lymphoma	4.636	0.3899

CNS, central nervous system.

phosphorylation were relatively more sensitive to PA4 treatment. When we measured the CAMKII γ activity among the 10 selected cell lines (Figure 3D), hematological cell lines, generally, had higher activation. Low levels of CAMKII γ activity in some PA4-responsive cell lines (MCF7, 786-O, and SKMEL2) suggested that PA4 might interfere with other kinases such as ZAP-70 (supplemental Figure 1C). The cytotoxicity of PA4 was specific for tumor cells; it did not affect healthy human peripheral blood mononuclear cells at therapeutic dosages (Figure 3E). These results demonstrated that PA4 exerted more profound cytotoxicity than BBM across the panel of cancer cell lines and preferentially targeted hematological cancers.

PA4 reduced c-Myc levels and induced ROS in lymphoma cells

Our previous work on BBM illustrated that it induced cell death by targeting the CAMKII γ -c-Myc axis.¹⁸ To investigate whether PA4 exerted tumor regression via the CAMKII γ -c-Myc axis, we performed the following experiments: first, the expression of CAMKII γ downstream proteins was examined by western blot after PA4 treatment. A considerable decrease in c-Myc was noticed with increasing

concentrations of PA4 in the T-cell lymphoma cell line H9 (supplemental Figure 2A). H9 cells with CAMKII γ knockout showed lower levels of c-Myc and were more resistant to PA4 treatment than without CAMKII γ knockout (supplemental Figure 2B). PA4 failed to reduce c-Myc levels in CAMKII γ -knockout cells (supplemental Figure 2C). These results unearthed that PA4 can selectively target CAMKII γ , thereby decreasing levels of c-Myc protein.

To further determine the underlying mechanisms of PA4-induced cell death, we compared the global gene profiles between vehicle control and 1 μ M PA4 treatment in H9 cells. Among the top pathways upregulated by PA4 treatments, we detected a significant increase in gene expressions from pathways related to cell death and cell cycle such as p53, apoptosis, and 1 point in the cell cycle from Gap2 phase to mitotic phase (G2M) checkpoint pathways (Figure 4A). The gene signature was similar to CAMK2G $^{-/-}$ primary T-cell lymphoma cells as observed in our previous study.¹⁸ Gene-set enrichment analysis showed that most Hallmark gene sets in CAMK2G $^{-/-}$ tumor were provoked toward upregulation (normalized enrichment score > 0). Among them, 29 Hallmark gene sets were consistently upregulated in both PA4-treated H9 cells and CAMK2G $^{-/-}$ T-cell lymphoma tumors (supplemental Figure 3A). Moreover, 4 of 6 pathways in Figure 4A (P53, apoptosis, reactive oxygen species (ROS) production, and hypoxia) were upregulated in CAMK2G $^{-/-}$ T-cell lymphoma tumors (supplemental Figure 3B). To determine whether PA4 treatment induced cell apoptosis, we stained cells with annexin V and analyzed them by flow cytometry. PA4 induced apoptosis in a dose-dependent manner (Figure 4B). Other apoptosis markers, such as cleaved poly-(adenosine 5'-diphosphate-ribose) polymerase and cleaved caspase 3, were also increased after PA4 treatment (Figure 4C), suggesting induction of an intrinsic apoptosis process. As expected, direct CAMKII γ gene knockout also resulted in similar apoptotic effects (Figure 4D), which can partially be rescued by reconstitution of CAMKII γ (supplemental Figure 4A).

Next, we investigated the underlying mechanisms by which PA4 induced cell apoptosis. Gene-set enrichment analysis suggested that unfolded protein response and ROS pathways were significantly induced after PA4 treatment (Figure 4A). Although physiological ROS work as cell-signaling molecules, excessive ROS, because of either more production or less detoxification, can damage cellular organelles and DNA, thereby inducing apoptosis and cell death.³⁶ To determine whether PA4 treatment elevated cellular ROS levels through CAMKII γ , we stained cells with fluorescent dyes 2',7'-dichlorodihydrofluorescein diacetate. Both PA4 treatment and CAMKII γ gene deletion increased intracellular ROS. In contrast, PA4 treatment in CAMKII γ -knockout cells did not exhibit higher ROS accumulation, indicating a CAMKII γ -dependent effect (Figure 4E; supplemental Figure 3C). Mitochondria and the endoplasmic reticulum (ER) are 2 major sources of intracellular ROS.³⁷ To distinguish the source of ROS, we stained the cells with MitoSOX, which is the specific dye for mitochondrial superoxide. Both PA4 treatment and CAMKII γ gene deletion induced mitochondrial superoxide accumulation (Figure 4E; supplemental Figure 3C). However, PA4 treatment in CAMKII γ -knockout cells still increased mitochondrial ROS, indicating that mitochondrial ROS accumulation by PA4 may not be induced through CAMKII γ inhibition alone. ROS induction by PA4 can be recapitulated in other lymphoma cell lines (supplemental Figure 3D). Treating cells with an antioxidant such as N-acetyl cysteine in addition to PA4

partially reduced the cytotoxicity and ROS production by PA4 (supplemental Figure 3E).

Unfolded protein response (UPR) was elevated after PA4 treatment, as illustrated by RNA sequencing (Figure 4A). UPR induces ER stress, which also coordinates with ROS to induce cell death.³⁸ Thus, we compared the ER stress markers before and after PA4 treatment (Figure 4F). PA4 treatment significantly increased protein kinase RNA-like ER kinase (PERK) phosphorylation, which further phosphorylated and activated the α subunit of the regulating initiator of the messenger RNA translation machinery (eIF2 α). The PERK-eIF2 α pathway then induced the transcription factor C/EBP homologous protein, which promotes oxidative stress in the ER and induces cell death.³⁹ Consistently, CAMKII γ -knockout cells demonstrated higher ER stress markers (Figure 4F), which were not further elevated by PA4 treatment, suggesting that CAMKII γ was required for the PA4-induced ER stress and subsequent ROS generation.

Taken together, by targeting CAMKII γ , PA4 not only reduced c-Myc protein levels but also elevated the levels of ROS, thereby increasing apoptosis.

PA4 effectively inhibited tumor growth in vivo

In our in vitro cancer cell line screening, PA4 produced the most cytotoxicity when administered to hematopoietic cancer cell lines. Accordingly, we chose to test the in vivo efficacy of PA4 using a lymphoma model. An H9-derived xenografted mouse model was established by inoculating 5×10^6 H9 cells subcutaneously in the flank of NSG mice. Xenografted tumors were allowed to reach a volume of 30 mm³ (day 16 after cell injection). Subsequently, mice were randomized into 5 groups: PBS, BBM, or 3 different escalated dosages of PA4 (Figure 5A). All treatments were administered daily via oral gavage for 14 days. The starting dosage of PA4 (5 mg/kg per day) was one-tenth of BBM (50 mg/kg per day) based on the in vitro IC₅₀ (Figure 2). Compared with BBM and PBS, treatment with PA4 significantly reduced tumor volume (Figure 5B-D). The in vivo efficacy of PA4 was also dose dependent; higher dosages of PA4 more dramatically reduced tumor growth. As with the PBS control, both BBM and PA4 did not reduce body weight (Figure 5E); these results suggested that both were well tolerated. Compared with the xenografted tumors from the PBS group, tumors from the PA4 group had lower levels of c-Myc (Figure 5F-G; supplemental Figure 5F).

In addition to assessing xenografted lymphomas, we also tested whether PA4 reduced tumors in vivo for nonhematopoietic cancers. The IC₅₀ of PA4 against multiple gastric cell lines was determined (supplemental Figure 5A-B). The SUN-1 cell line was selected and inoculated subcutaneously to NSG mice. After allowing the tumor to establish for 7 days, the mice were treated with control (PBS), BBM, or PA4. Although PA4 significantly impaired tumor growth (vs PBS) in the gastric cancer model (supplemental Figure 5C-E), it was less pronounced than in the lymphoma model. This in vivo result also supported the in vitro toxicity result that PA4 was more specific to hematopoietic cancers.

Collectively, targeting CAMKII γ via PA4 may be a reasonable therapeutic strategy for treating hematopoietic cancers.

Pharmacokinetic study of PA4

To assess how PA4 was distributed after a 14-day oral gavage, we measured PA4 concentrations in both serum and tumor tissues.

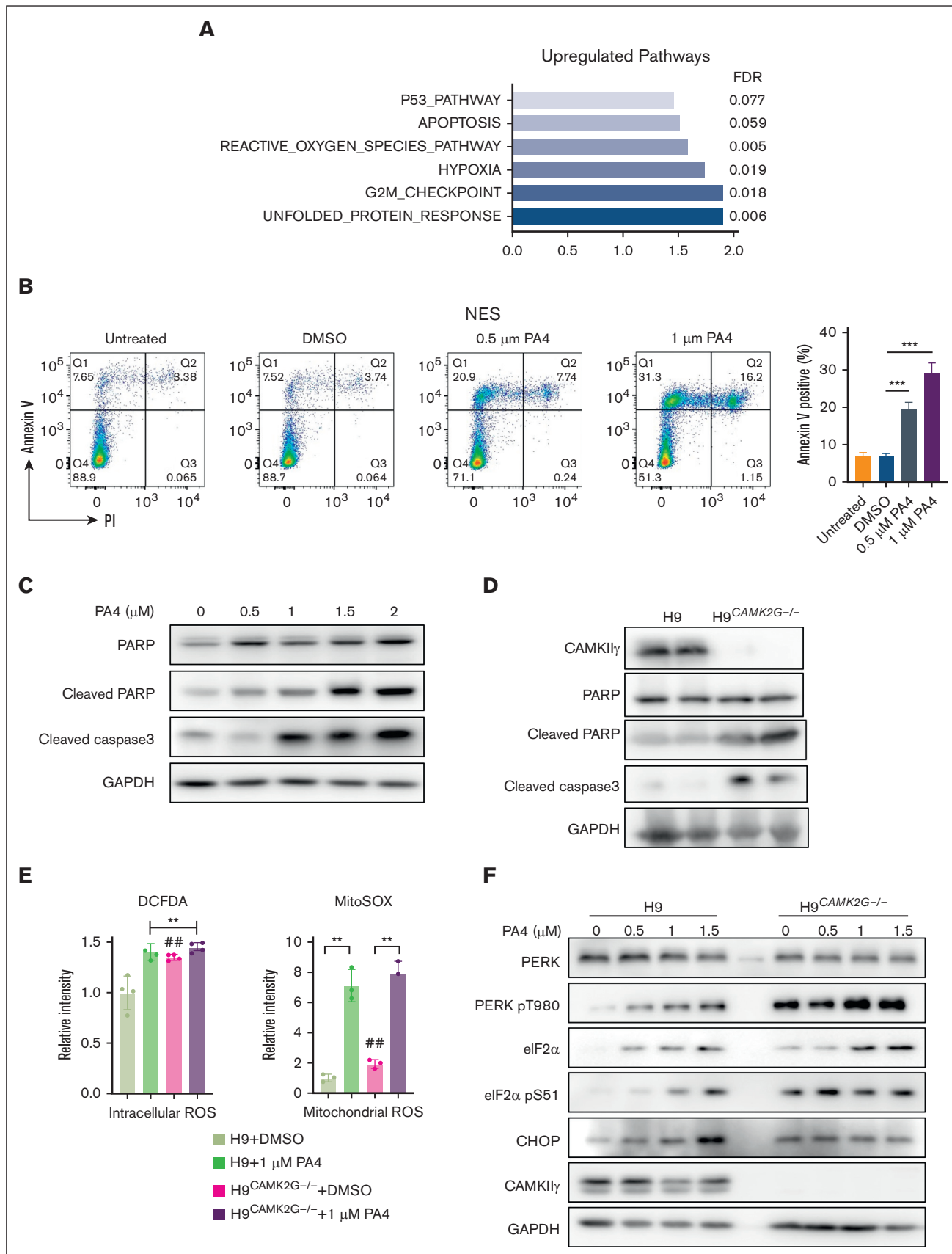


Figure 4.

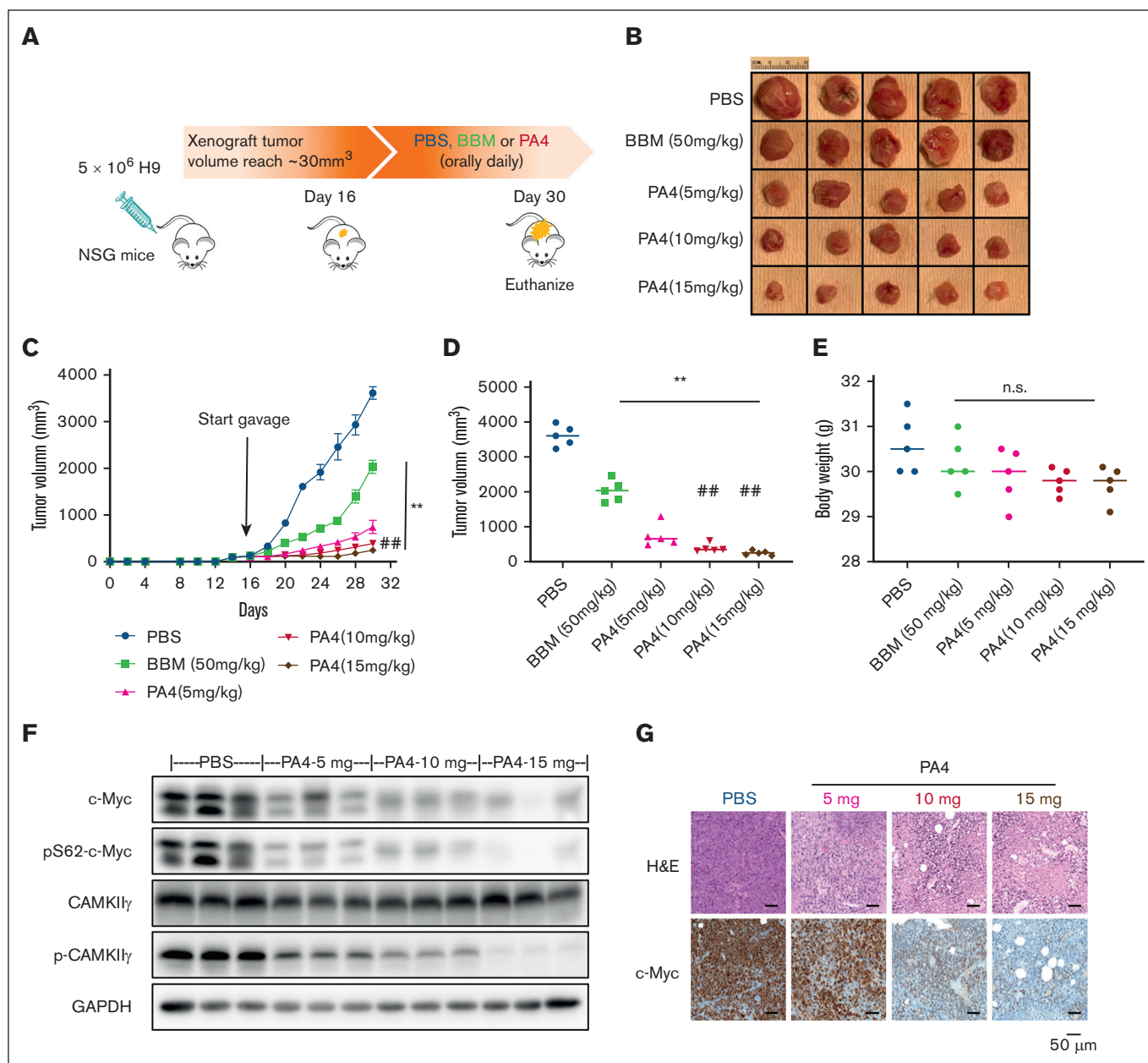


Figure 5. PA4 inhibits tumor growth in vivo. (A) Scheme of H9-induced lymphoma in NSG mouse model, and pharmacological inhibition by PA4. Representative images of tumors (B) and tumor growth curve (C) of NSG mice treated with either PBS, BBM, or PA4. (D) Tumor size at end point of the 30th day. ****** $P < .01$ vs PBS group; **##** $P < .01$ vs PA4 5-mg/kg group. (E) Body weight of mice in indicated groups. No statistical significance (ns) vs PBS group. (F) Representative western blot analysis of CAMK1 γ and c-Myc protein in tumor tissues from PA4 and PBS groups. GAPDH is used as loading control. (G) Representative images of hematoxylin and eosin (H&E) and immunohistochemical staining of c-Myc with sections of tumors from PA4 and PBS groups.

Figure 4. PA4 enhances ROS generation to induce lymphoma cell apoptosis. (A) Summary of gene-set enrichment analysis reveals the overrepresentation of indicated pathways in PA4 treated group. Genes are ranked into an ordered list based on relative expression in control and PA4-treated H9 cells. (B) Cells were treated with indicated dosages of PA4 for 24 hours and stained with annexin V and 4',6-diamidino-2-phenylindole for apoptosis analysis. Data are shown as mean \pm SD, $n = 3$. ****** $P < .01$ vs DMSO treatment (C) and H9 wild-type and H9^{CAMK2G^{-/-}} cells (D). (E) Cells were treated with DMSO or 1 μ M PA4 for 24 hours and stained with 2',7'-dichlorodihydrofluorescein diacetate (H₂DCFH-DA) for intracellular ROS, and MitoSOX for mitochondrial superoxide analysis. Data are shown as mean \pm SD, $n = 3$. ****** $P < .01$ and **##** $P < .01$ vs H9 + DMSO treatment. (F) Representative western blots for ER stress markers after PA4 treatment in wild-type H9 and H9^{CAMK2G^{-/-}} cells for 24 hours. CHOP, C/EBP homologous protein; FDR, false discovery rate; G2M, cell cycle 2 phase to M phase transition; PARP, poly-(adenosine 5'-diphosphate-ribose) polymerase.

Increasing oral dosages of PA4 led to increased accumulation in both serum and tumor tissues (Figure 6A).

We compared the pharmacokinetics of BBM with that of PA4. Male Institute of Cancer Research mice were administered with either BBM or PA4 at the same concentration. We assessed both IV and oral routes of administration. The plasma concentrations vs time point profiles are shown in Figure 6B. Both BBM and PA4 were rapidly absorbed into the blood and detected 5 minutes after oral administration. PA4 displayed a higher area under the curve than BBM (28704 ± 1951 vs 8478 ± 1150). The absolute oral bioavailability of PA4 was lower than BBM (34.1% vs 44.8%). This might have been due to the slower elimination of PA4 after both IV and oral administration (Figure 6B), which led to compound accumulation in a short period. The relatively long half-life of PA4 suggested that longer dose intervals should be considered for future application. Results from stability studies on both BBM and PA4 indicated that they were stable during both the sample preparation and subsequent analyses (supplemental Table 1).

To monitor the dynamics and clearance of PA4 in the blood, we measured serum PA4 levels from the mice after they received 1 of the following regimens: 2 weeks of PA4, 4 weeks of PA4, or 2 weeks of PA4 followed by 2 weeks without treatment. Longer oral dosing did not result in long-term PA4 accumulation in the serum. Minimal PA4 was detected 2 weeks after treatment ceased (Figure 6C).

Safety assessment of PA4

We assessed PA4 in both short-term single-dose studies and longer-term studies. To measure the acute systemic toxicity of PA4, CD-1 mice were treated orally with 1 of the following doses as a single dose: 5 mg/kg, 15 mg/kg, 30 mg/kg, and 50 mg/kg (Figure 7A). After 14 days, there were no mortalities. By the end of the study, all animals had gained weight (Figure 7B). No abnormalities were observed in any of the tested animals in gross necropsy.

We performed longer-term toxicity testing using 8-week-old C57BL/6j mice (Figure 7C). The mice received oral gavage with 50 mg/kg PA4 daily for 12 consecutive days (n = 6). After 12 days, there were no mortalities and no significant reductions in body weight (Figure 7D). Serum alanine aminotransferase and aspartate aminotransferase levels suggest that this regimen of PA4 did not cause liver damage (Figure 7E). High dosage of PA4 treatment also did not cause organ damage as shown by the morphology of major organs in mice (Figure 7F).

Discussion

Considering the emerging roles that CAMKII plays in serious diseases, a wealth of basic research has been aimed at developing pharmacological inhibitors. Efforts to translate CAMKII inhibitor use to the clinic have yielded some new compounds, including

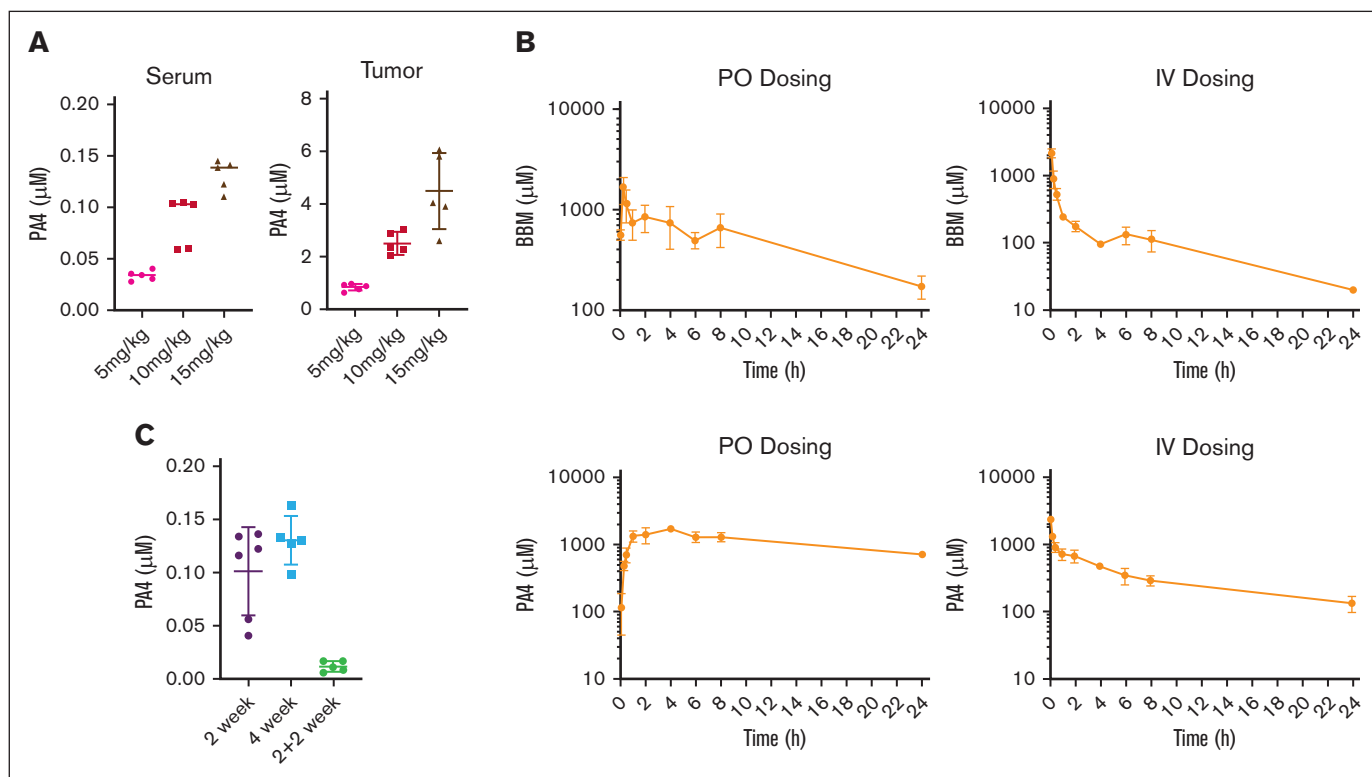


Figure 6. Mouse pharmacokinetic study of PA4. (A) PA4 concentration in serum and tumor tissues after the 14 day PA4 treatment in NSG mice shown in Figure 5. Data are shown as mean with SD. (B) Mean plasma concentration-time profiles of BBM (top) and PA4 (bottom) in Institute of Cancer Research mice after IV and oral administrations (n = 3). (C) PA4 concentration in serum from mice that received oral gavage with PA4 for 2 weeks, 4 weeks, or 2 weeks plus 2 weeks without treatment.

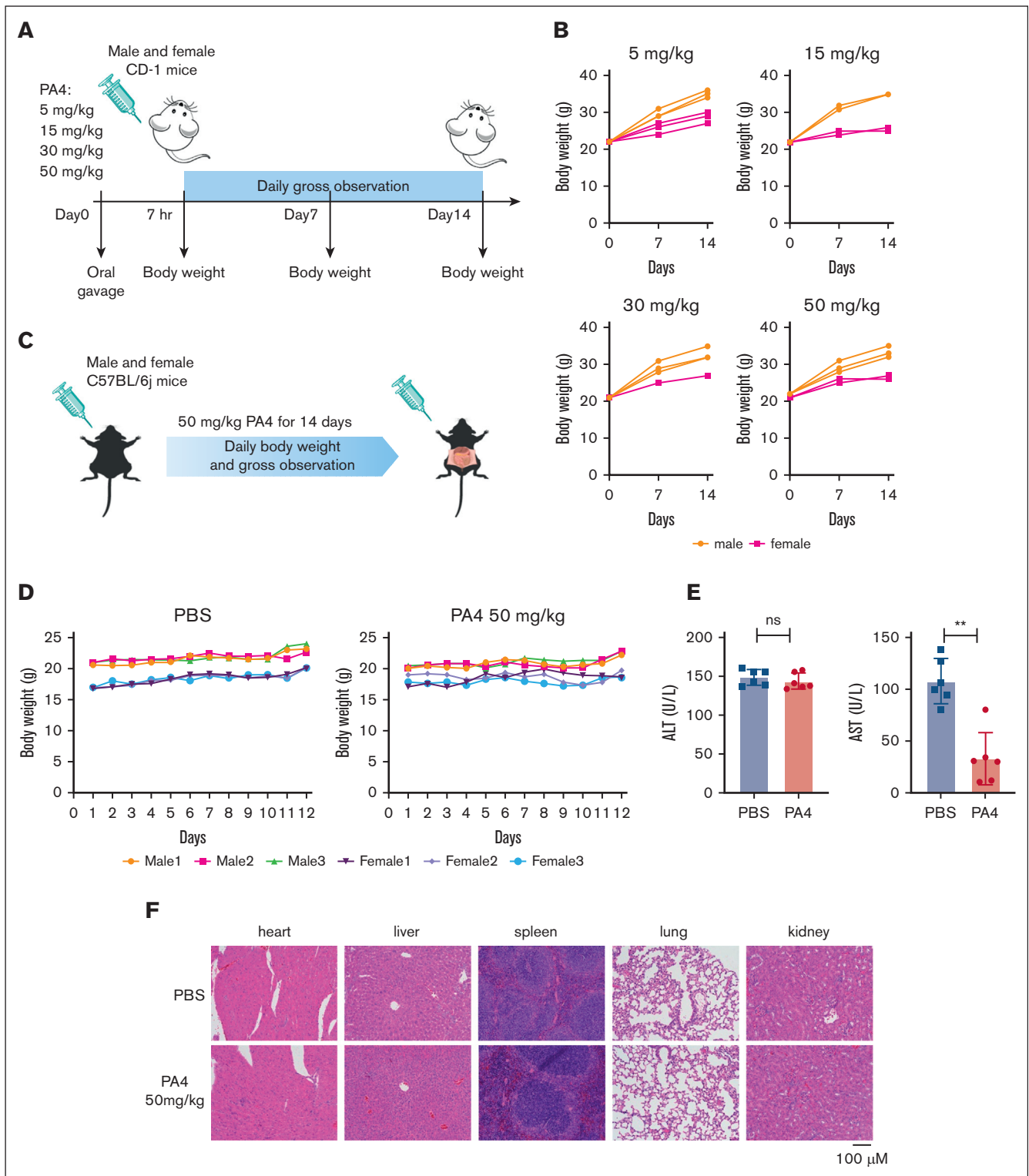


Figure 7. Mouse pilot toxicity study of PA4. (A) Scheme of short-term safety assessment in CD-1 mice. (B) Body weight of CD-1 mice after being orally administrated with indicated dosages of PA4 once. (C) Scheme of subacute toxicity assessment in C57BL/6j mice. (D) Body weight of mice during oral gavage with PBS or 50mg/kg PA4 daily for 12 days. (E) Serum alanine aminotransferase (ALT) and aspartate aminotransferase (AST) levels after 12-day 50-mg/kg PA4 treatment; $**P < .01$. (F) Representative images of H&E staining of indicated organs from PA4 and PBS treatment groups.

pyrimidines (Scios 15b, AS105),^{24,40} 4-azabenzimidazoles (GS-680),²⁵ and thienopyrimidines (RA306).⁴¹ Our group previously identified BBM as a specific CAMKII γ inhibitor that effectively inhibited T-cell lymphomagenesis.¹⁸ Using BBM as the starting point, we synthesized a novel BBM derivative, PA4. Through a combination of biophysics and ex vivo assays, we have determined that both the specificity and the potency of PA4 as a CAMKII γ inhibitor are strongly improved compared with its parent compound BBM.

Furthermore, by taking advantage of PA4 with much higher potency to inhibit CAMKII γ , we were able to determine additional molecular mechanisms by which PA4 inhibited T-cell lymphoma. In addition to the suppression of the CAMKII γ -c-Myc axis, we identified a new mechanism by which PA4 induces cell apoptosis via UPR-ROS production. Increased ROS is a double-edged sword for cancers; it promotes tumorigenic signaling at the cancer initiation stage but also triggers cell death throughout cancer development.^{42,43} Rapid turnover of cancer cells induces stress in ER protein folding, assembly, and transport, resulting in the accumulation of unfolded or misfolded proteins and the activation of the UPR pathways. ROS can be generated after ER stress as a byproduct of oxidative proteins. This production of ROS from UPR is also CAMKII γ dependent and different from the ROS generated by mitochondria (Figure 4E). Because dysregulation of UPR and ROS are common in many tumors, further studies of PA4 and these pathways may be applied to other tumors.

Although PA4 demonstrated the strongest inhibition of CAMKII γ , it also showed significant inhibition of CAMKII δ . Because different isoforms of 1 protein family could, to some extent, compensate for each other functionally,^{44,45} a dual inhibitor for both isoforms may achieve better efficacy. In a previous publication,³⁴ we found that both CAMKII γ and CAMKII δ were coexpressed and were important in the promotion of the growth of aggressive B-cell lymphomas such as double-hit lymphoma. PA4 treatment demonstrated good therapeutic efficacy by inhibiting both isoforms.

Like CAMKII γ , CAMKII δ also has a broad expression among multiple tissues, but its potential role in cancer still needs more investigation. Interestingly, a previous report has indicated that both CAMKII γ and CAMKII δ may form a synthetic lethality relationship with c-MYC in cancer cells.⁴⁶ This suggests that CAMKII inhibition can be an alternative approach to bypass direct c-Myc targeting and achieve therapeutic effects in c-MYC-driven cancers. Another potential advantage to treat c-Myc-dependent cancer by targeting its synthetic lethality with CAMKII is its selectivity toward cancer cells, sparing healthy cells without this synthetic lethality relationship. Because lymphoma cells generally have higher c-Myc expression levels and activation, PA4 is expected to have a more potent effect on lymphoma compared with other kinds of cancer by targeting 2 CAMKII isoforms.

To go a step further, we measured both pharmacokinetic parameters and safety of PA4 in mice. It was rapidly absorbed (<5 minutes) and exhibited long retention (half-life > 24 hours). Despite the slow elimination of PA4, prolonged oral dosing of PA4 did not further increase the PA4 accumulation in the blood (Figure 6C). These results suggest that PA4 can achieve a steady

state in the blood after oral dosing. Considering that the half-life of PA4 in plasma was longer than 24 hours, future studies with PA4 may use a longer dosing interval.

In conclusion, tolerable dosing regimens of PA4 produced marked antilymphoma activity in both in vitro and in vivo models of lymphoma. Its efficacy, safety, and favorable pharmacokinetic profile support PA4 as a potential candidate to treat lymphomas and other cancers.

Acknowledgments

The authors are grateful to Michael Kahn and Lili Wang from City of Hope for their discussion and advice. The authors acknowledge Christoph Pittius and Mingyue Zhou at City of Hope for their insightful input. The authors thank Ian Talisman from City of Hope for his help in manuscript editing and proofreading. The authors appreciate Xuxiang Liu from City of Hope for providing human peripheral blood mononuclear cells.

W.H. is supported by National Cancer Institute award number NCI 2R01CA139158 and National Institute of Diabetes and Digestive and Kidney Diseases award number NIDDK R01DK124627. Research reported in this publication was also supported by National Cancer Institute of the National Institutes of Health award number P30CA33572 and City of Hope Integrated Drug Development Venture.

Authorship

Contribution: W.H. designed and supervised most of the experiments; S.X. performed most of the experiments and data analysis and wrote the manuscript; S.W., M.Z., Y.W., J.W., and M.F. contributed to the H9-NSG mice experiments; M.L. contributed to the SUN-1 NSG mice experiments; J.X. synthesized BBM and PA4; H.Y. and D.K. performed experiments on NCI-60 cell line profiling; C.O. and X.W. conducted RNA sequencing analysis; J.Z., Z.F., H.C., J.H., and W.L. provided technical assistance for some experiments; Z.L. and J.M. helped analyze the public data set; N.Q. and L.J. helped edit the manuscript; and D.H. and W.C.C. provided conceptual and technical advice, as well as overall support.

Conflict-of-interest disclosure: The authors declare no competing financial interests.

ORCID profiles: L.J., 0000-0002-2685-6048; Z.F., 0000-0001-5720-1709; C.O., 0000-0002-7452-2800; Z.L., 0000-0002-2220-8430; J.M., 0000-0002-7065-9666; W.H., 0000-0003-3735-9466.

Correspondence: David Horne, Department of Molecular Medicine, Beckman Research Institute, City of Hope National Medical Center, 1500 Duarte Rd, Duarte, CA 91010; email: dhorne@coh.org; and Wendong Huang, Molecular and Cellular Biology of Cancer Program and Department of Diabetes Complications and Metabolism, Arthur Riggs Diabetes and Metabolic Research Institute, Beckman Research Institute, City of Hope National Medical Center, Duarte Rd, Duarte, CA 91010; email: whuang@coh.org.

References

1. Hudmon A, Schulman H. Structure–function of the multifunctional Ca²⁺/calmodulin-dependent protein kinase II. *Biochem J*. 2002;364(Pt 3):593-611.
2. Tobimatsu T, Fujisawa H. Tissue-specific expression of four types of rat calmodulin-dependent protein kinase II mRNAs. *J Biol Chem*. 1989;264(30):17907-17912.
3. He Q, Li Z. The dysregulated expression and functional effect of CaMK2 in cancer. *Cancer Cell Int*. 2021;21(1):326.
4. Si J, Collins SJ. Activated Ca²⁺/calmodulin-dependent protein kinase II γ is a critical regulator of myeloid leukemia cell proliferation. *Cancer Res*. 2008;68(10):3733-3742.
5. Skelding KA, Rostas JAP, Verrills NM. Controlling the cell cycle: the role of calcium/calmodulin-stimulated protein kinases I and II. *Cell Cycle*. 2011;10(4):631-639.
6. Jing Z, Sui X, Yao J, et al. SKF-96365 activates cytoprotective autophagy to delay apoptosis in colorectal cancer cells through inhibition of the calcium/CaMKII γ /AKT-mediated pathway. *Cancer Lett*. 2016;372(2):226-238.
7. Yuan K, Chung LWK, Siegal GP, Zayzafoon M. α -CaMKII controls the growth of human osteosarcoma by regulating cell cycle progression. *Lab Invest*. 2007;87(9):938-950.
8. Bourguignon LYW, Gilad E, Brightman A, Diedrich F, Singleton P. Hyaluronan-CD44 interaction with leukemia-associated RhoGEF and epidermal growth factor receptor promotes rho/ras co-activation, phospholipase C ϵ -Ca²⁺ signaling, and cytoskeleton modification in head and neck squamous cell carcinoma cells. *J Biol Chem*. 2006;281(20):14026-14040.
9. Britschgi A, Bill A, Brinkhaus H, et al. Calcium-activated chloride channel ANO1 promotes breast cancer progression by activating EGFR and CAMK signaling. *Proc Natl Acad Sci U S A*. 2013;110(11):E1026-E1034.
10. Meng Z, Li T, Ma X, et al. Berbamine inhibits the growth of liver cancer cells and cancer-initiating cells by targeting Ca²⁺/calmodulin-dependent protein kinase II. *Mol Cancer Therapeut*. 2013;12(10):2067-2077.
11. Ma X, Meng Z, Jin L, et al. CAMK2 γ in intestinal epithelial cells modulates colitis-associated colorectal carcinogenesis via enhancing STAT3 activation. *Oncogene*. 2017;36(28):4060-4071.
12. Shin HJ, Lee S, Jung HJ. A curcumin derivative hydrazinobenzoylcurcumin suppresses stem-like features of glioblastoma cells by targeting Ca²⁺/calmodulin-dependent protein kinase II. *J Cell Biochem*. 2019;120(4):6741-6752.
13. Chai S, Xu X, Wang Y, et al. Ca²⁺/calmodulin-dependent protein kinase II γ enhances stem-like traits and tumorigenicity of lung cancer cells. *Oncotarget*. 2015;6(18):16069-16083.
14. Li N, Jiang P, Du W, et al. Siva1 suppresses epithelial-mesenchymal transition and metastasis of tumor cells by inhibiting stathmin and stabilizing microtubules. *Proc Natl Acad Sci U S A*. 2011;108(31):12851-12856.
15. Li J, Zheng C, Wang M, et al. ROS-regulated phosphorylation of ITPKB by CAMK2G drives cisplatin resistance in ovarian cancer. *Oncogene*. 2022;41(8):1114-1128.
16. Gu Y, Chen T, Meng Z, et al. CaMKII γ , a critical regulator of CML stem/progenitor cells, is a target of the natural product berbamine. *Blood*. 2012;120(24):4829-4839.
17. Jiang X, Wu Z, Lu X, et al. Activation of CaMKII γ ; potentiates T-cell acute lymphoblastic leukemia leukemogenesis via phosphorylating FOXO3a. *Oncotarget*. 2017;8(43):75050-75064.
18. Gu Y, Zhang J, Ma X, et al. Stabilization of the c-Myc protein by CAMKII γ promotes T cell lymphoma. *Cancer Cell*. 2017;32(1):115-128.e7.
19. Bui JD, Calbo S, Hayden-Martinez K, Kane LP, Gardner P, Hedrick SM. A role for CaMKII in T cell memory. *Cell*. 2000;100(4):457-467.
20. Rosenberg OS, Deindl S, Sung R-J, Nairn AC, Kuriyan J. Structure of the autoinhibited kinase domain of CaMKII and SAXS analysis of the holoenzyme. *Cell*. 2005;123(5):849-860.
21. Hanson PI, Meyer T, Stryer L, Schulman H. Dual role of calmodulin in autophosphorylation of multifunctional cam kinase may underlie decoding of calcium signals. *Neuron*. 1994;12(5):943-956.
22. Lai Y, Nairn AC, Greengard P. Autophosphorylation reversibly regulates the Ca²⁺/calmodulin-dependence of Ca²⁺/calmodulin-dependent protein kinase II. *Proc Natl Acad Sci U S A*. 1986;83(12):4253-4257.
23. Sumi M, Kiuchi K, Ishikawa T, et al. The newly synthesized selective Ca²⁺/calmodulin dependent protein kinase II inhibitor KN-93 reduces dopamine contents in PC12h cells. *Biochem Biophys Res Commun*. 1991;181(3):968-975.
24. Neef S, Steffens A, Pellicena P, et al. Improvement of cardiomyocyte function by a novel pyrimidine-based CaMKII-inhibitor. *J Mol Cell Cardiol*. 2018;115:73-81.
25. Lebek S, Plöbl A, Baier M, et al. The novel CaMKII inhibitor GS-680 reduces diastolic SR Ca leak and prevents CaMKII-dependent pro-arrhythmic activity. *J Mol Cell Cardiol*. 2018;118:159-168.
26. Nassal D, Gratz D, Hund TJ. Challenges and opportunities for therapeutic targeting of calmodulin kinase II in heart. *Front Pharmacol*. 2020;11:11.
27. Xie J, Ma T, Gu Y, et al. Berbamine derivatives: a novel class of compounds for anti-leukemia activity. *Eur J Med Chem*. 2009;44(8):3293-3298.
28. Yang F, Nam S, Brown CE, et al. A novel berbamine derivative inhibits cell viability and induces apoptosis in cancer stem-like cells of human glioblastoma, via up-regulation of miRNA-4284 and JNK/AP-1 signaling. *PLoS One*. 2014;9(4):e94443.

29. Yang F, Nam S, Zhao R, et al. A novel synthetic derivative of the natural product berbamine inhibits cell viability and induces apoptosis of human osteosarcoma cells, associated with activation of JNK/AP-1 signaling. *Cancer Biol Ther.* 2013;14(11):1024-1031.
30. Shen J-K, Du H-P, Ma Q, Yang M, Wang Y-G, Jin J. 4-Chlorobenzoyl berbamine, a novel berbamine derivative, induces apoptosis in multiple myeloma cells through the IL-6 signal transduction pathway and increases FOXO3a-Bim expression. *Oncol Rep.* 2013;30(1):425-432.
31. Jafari R, Almqvist H, Axelsson H, et al. The cellular thermal shift assay for evaluating drug target interactions in cells. *Nat Protoc.* 2014;9(9):2100-2122.
32. Anastassiadis T, Deacon SW, Devarajan K, Ma H, Peterson JR. Comprehensive assay of kinase catalytic activity reveals features of kinase inhibitor selectivity. *Nat Biotechnol.* 2011;29(11):1039-1045.
33. Nepali K, Lee H-Y, Liou J-P. Nitro-group-containing drugs. *J Med Chem.* 2019;62(6):2851-2893.
34. Liu X, Xu S, Zhang J, et al. Targeting MYC and BCL2 by a natural compound for "double-hit" lymphoma. *Hematol Oncol.* 2022;40(3):356-369.
35. Liu Y, Wang X, Deng L, et al. ITK inhibition induced in vitro and in vivo anti-tumor activity through downregulating TCR signaling pathway in malignant T cell lymphoma. *Cancer Cell Int.* 2019;19:32.
36. Auten RL, Davis JM. Oxygen toxicity and reactive oxygen species: the devil is in the details. *Pediatr Res.* 2009;66(2):121-127.
37. Yoboue ED, Sitia R, Simmen T. Redox crosstalk at endoplasmic reticulum (ER) membrane contact sites (MCS) uses toxic waste to deliver messages. *Cell Death Dis.* 2018;9(3):331.
38. Bhattarai KR, Riaz TA, Kim H-R, Chae H-J. The aftermath of the interplay between the endoplasmic reticulum stress response and redox signaling. *Exp Mol Med.* 2021;53(2):151-167.
39. Marciniak SJ, Yun CY, Oyamomari S, et al. CHOP induces death by promoting protein synthesis and oxidation in the stressed endoplasmic reticulum. *Genes Dev.* 2004;18(24):3066-3077.
40. Mavunkel B, Xu YJ, Goyal B, et al. Pyrimidine-based inhibitors of CaMKII δ . *Bioorg Med Chem Lett.* 2008;18(7):2404-2408.
41. Beauverger P, Ozoux ML, Bégis G, et al. Reversion of cardiac dysfunction by a novel orally available calcium/calmodulin-dependent protein kinase II inhibitor, RA306, in a genetic model of dilated cardiomyopathy. *Cardiovasc Res.* 2020;116(2):329-338.
42. Reczek CR, Chandel NS. The two faces of reactive oxygen species in cancer. *Annu Rev Cell Biol.* 2017;1(1):79-98.
43. Perillo B, Di Donato M, Pezone A, et al. ROS in cancer therapy: the bright side of the moon. *Exp Mol Med.* 2020;52(2):192-203.
44. Li X, Mazaleuskaya LL, Yuan C, et al. Flipping the cyclooxygenase (Ptgs) genes reveals isoform-specific compensatory functions^{1,2}[S]. *JLR (J Lipid Res).* 2018;59(1):89-101.
45. Sellers JR, Heissler SM. Nonmuscle myosin-2 isoforms. *Curr Biol.* 2019;29(8):R275-R278.
46. Toyoshima M, Howie HL, Imakura M, et al. Functional genomics identifies therapeutic targets for MYC-driven cancer. *Proc Natl Acad Sci U S A.* 2012;109(24):9545-9550.